

# A Fully Traceless Cartesian Multipole Formulation for the Distributed Fast Multipole Method

Jonathan P. Coles<sup>a,\*</sup>, Rebekka Bieri<sup>b</sup>

<sup>a</sup>Physik-Department T38, Technische Universität München, James-Frank-Str. 1, D-85748 Garching, Germany

<sup>b</sup>Max Planck Institute for Astrophysics, Karl-Schwarzschild-Str. 1, D-85741 Garching, Germany

## Abstract

We present efficient operators for the fast multipole method (FMM) based on totally symmetric and traceless Cartesian multipole tensors, which have been designed to translate well into computer code. Using the traceless tensor form significantly reduces memory usage and network communication traffic for large-scale applications in molecular dynamics and astrophysics. We have also developed a software generator that symbolically produces, verifies, and optimizes code for the FMM operators. The generator can easily produce different forms of the operators more suitable to specific applications. In realistic tests of biophysical simulations we observe a 20% speed-up, demonstrating the efficiency and improved performance of these routines compared to non-traceless tensor operators.

*Keywords:* Fast multipole method, numerical methods, N-body simulations

## 1. Introduction

The behavior of many physical systems can be described by a potential function  $\Phi \sim 1/R$  that scales inversely as a function of distance. For systems modeled as a collection of  $N$  discrete particles, this function acts between pairs of particles, resulting in  $O(N^2)$  interactions. An exact calculation of  $\Phi$  quickly becomes prohibitive on modern hardware even for modestly sized problems of several thousand particles. Furthermore, following the time evolution of the particles requires  $\nabla\Phi$  to be computed thousands if not millions of times. In the fields of molecular dynamics and astrophysics many approximate methods have been developed to make their respective problems tractable. Popular methods include the Barnes-Hut tree code (Barnes and Hut, 1986) which scales as  $O(N \log N)$ ; Particle Mesh Ewald (PME, Darden et al. (1993)), a spectral method which also scales as  $O(N \log N)$  but implicitly handles periodic boundary conditions; and the Fast Multipole Method (FMM) (Greengard and Rokhlin, 1987), which has a scaling of just  $O(N)$ .

The theoretical scaling of FMM is clearly computationally attractive and from a physical point of view, the multipole expansion approach is simple to understand. The method approximates sub-regions of the simulation volume by multipole expansions of the local sources (typically represented as discrete point particles) and computes the effect of one entire region on another. The FMM approach also requires less network communication when used in a distributed computing environment; a feature that is becoming more important as we approach the era of exascale machines (Yokota and Barba, 2012).

However, developing an efficient FMM implementation still requires a significant investment of time and understanding. In fact, there is no single FMM formalism and the specifics often depend on the problem at hand.

Originally, FMM was developed using spherical harmonics, which give the multipoles a simple representation. In terms of the expansion order  $p$ , the number of floating-point operations (FLOPs) scales as  $O(p^4)$  and requires storing  $O(p^2)$  expansion coefficients. Later developments by the same authors using planewaves reduced the FLOP scaling to  $O(p^3)$  (Greengard and Huang, 2002).

The multipole expansion can also be expressed in the Cartesian basis set, which avoids trigonometric functions and the conversion of coordinates for applications already using a Cartesian basis. The greatest disadvantage, however, is that a straightforward implementation scales as  $O(p^6)$  and stores  $\binom{p+3}{2}$  coefficients because of the introduction of many extraneous dependent terms in the multipole tensors. For many applications, this is not a serious problem as the expansion is often restricted to  $2 \leq p \leq 5$ . Using a Cartesian form of spherical harmonics, (Dehnen, 2014) demonstrated a method that scales as  $O(p^3)$  and was faster for  $p \geq 5$  and reduces the number of stored coefficients. For implementations of FMM that run on large, distributed computers, the number of stored coefficients can have a significant impact on performance as the multipole expansion coefficients for interacting regions must often be copied between machines.

At each order of the expansion  $n \leq p$ , the  $n$ -rank Cartesian multipole tensor  $\mathbf{M}^{(n)}$  carries  $\binom{n+2}{2}$  terms (for  $n = p = 7$ , there are 36 coefficients). The equivalent spherical harmonics only need  $2n + 1$  terms per rank. Nearly three decades ago Appleq-

\*Corresponding author

Email addresses: jonathan.coles@tum.de (Jonathan P. Coles), bieri@mpa-garching.mpg.de (Rebekka Bieri)

uist (1989) discussed the intimate relationship between spherical harmonics and the traceless form of a Cartesian position tensor and provided a detracer operator to convert any totally symmetric tensor into a totally symmetric *traceless* tensor. In a traceless tensor, many components become redundant and recasting Cartesian tensors in a traceless form only requires storing a total of  $(p + 1)^2$  terms. For our applications to molecular dynamics, this represents a savings of 47% (see Table B.3 in the appendix).

Using the detracer, Shanker and Huang (2007) derived equations for computing FMM interactions with traceless tensors, but the multipole shifting operator (which we will present later) does not actually yield another traceless multipole, making the method incomplete. More recent work by some of the same authors does not use the detracer, but instead takes advantage of the traceless nature of the harmonic gradient operator for  $1/r$  to improve the computational efficiency (Huang et al., 2018). In Lorenzen et al. (2012), the authors present a complete traceless treatment of the FMM equations, but do not use an efficient form of the gradient operator as shown in Applequist (1989). Furthermore, the given equations are not in a form that translates easily into computer software.

In this paper, we bring together an efficient formulation of the FMM equations in the Cartesian basis using only traceless tensors, including the gradient operator, and in a form that translates well into computer code. We also have developed a software tool based on a symbolic algebra library to automatically generate, and optimize, the code for any target computer language. The optimization process is able to perform tedious subexpression elimination, which significantly reduces the total number of mathematical operations in the resulting code. Furthermore, we can symbolically verify the correctness of the expressions. The resulting computer functions are currently employed in the highly parallelized molecular dynamics software Polaris(MD) (Masella et al., 2008, 2011, 2013).

In Sec. 2 we review the mathematical tools for handling traceless Cartesian tensors and apply it to developing the physical theory behind the fast multipole method in Sec. 3. In Sec. 4 we rewrite these operators in a more efficient form and discuss higher order applications and a tool for automatically generating optimized computer code. We review the actual FMM algorithm we employ in Sec. 6. Our comparison results using the new traceless multipole operators are presented in Sec. 7. Finally, we summarize our findings in the Sec. 8.

## 2. Mathematical Background

In this section we present the necessary formalisms for traceless tensors, following the work of Applequist (1989), which contains full proofs and additional details. In the three dimensional Cartesian basis, an  $n$ -rank tensor  $\mathbf{A}^{(n)}$  contains  $3^n$  elements. If the tensor is symmetric (which we will assume here) only the upper triangle of the tensor is necessary. We can store the remaining  $(n + 1)(n + 2)/2$  elements in a *compressed form* where an element is  $A^{(n)}(n_1, n_2, n_3)$ . The polytensor  $\mathbf{A} = \{\mathbf{A}^{(0)}, \mathbf{A}^{(1)}, \mathbf{A}^{(2)}, \dots\}$  is a set of tensors of increasing

rank that will be used to store the tensors of multipole moment expansion used by the fast multipole method.

We simplify the notation using the multi-index tuple  $\mathbf{n} = (n_1, n_2, n_3)$ , where  $|\mathbf{n}| = n = n_1 + n_2 + n_3$  and  $n_i \geq 0$ . This index naturally captures the compressed format so we may write  $\mathbf{A}_{\mathbf{n}}^{(n)} \equiv A^{(n)}(n_1, n_2, n_3)$ . If we leave out the superscript as in  $\mathbf{A}_{\mathbf{n}}$  we mean the element  $\mathbf{n}$  in the tensor  $\mathbf{A}^{(n)}$  in the polytensor  $\mathbf{A}$ . See Sec. Appendix A for a further explanation of the multi-index notation.

We define  $\mathbf{C}^{(m)} = \mathbf{A}^{(m+n)} \cdot \mathbf{n} \cdot \mathbf{B}^{(n)}$  to be the  $n$ -fold contraction of two tensors. The contraction can be computed as

$$\mathbf{C}_{\mathbf{m}}^{(m)} = \sum_{|\mathbf{k}|=n} \frac{n!}{\mathbf{k}!} \mathbf{A}_{\mathbf{m}+\mathbf{k}}^{(m+n)} \mathbf{B}_{\mathbf{k}}^{(n)} \quad (1)$$

where the summation is over all possible values of  $\mathbf{k}$  such that  $|\mathbf{k}| = n$ . While the contraction  $\mathbf{A}^{(m+n)} \cdot \mathbf{n} \cdot \mathbf{B}^{(n)}$  produces a tensor of reduced rank  $m$ , the direct product (also known as a Kronecker product)  $\mathbf{C}^{(m+n)} = \mathbf{A}^{(m)} \mathbf{B}^{(n)}$  is a  $(m + n)$ -rank tensor. The direct product of  $n$  copies of a vector is a symmetric  $n$ -rank tensor. For a vector  $\mathbf{r}$ , when we write  $r_{\mathbf{n}}^k$  we mean the  $\mathbf{n}$ th element of the tensor  $\mathbf{r}^k$ .

It is important to state that the direct product between two symmetric tensors is not, in general, symmetric and cannot be represented using the multi-index notation (consider for example the simple direct product of  $[x, y][a, b] = [[xa, xb], [ya, yb]]$ ). For symmetric tensors  $\mathbf{A}^{(m)}, \mathbf{B}^{(n-m)}$  the symmetric direct product  $\text{Sym}(\mathbf{C}^{(n)}) = \mathbf{A}^{(m)} \mathbf{B}^{(n-m)}$  using the multi-index notation is

$$\text{Sym}(\mathbf{C}_{\mathbf{n}}^{(n)}) = \sum_{|\mathbf{k}|=|\mathbf{n}|} \frac{k! (n-k)!}{\mathbf{k}! (\mathbf{n}-\mathbf{k})!} \frac{\mathbf{n}!}{n!} \mathbf{A}_{\mathbf{k}}^{(m)} \mathbf{B}_{\mathbf{n}-\mathbf{k}}^{(n-m)} \quad (2)$$

The trace in one index pair of a tensor  $\mathbf{A}^{(n)}$  is a reduced tensor of rank  $k = n - 2$  and is defined to be  $\mathbf{A}_{\mathbf{k}}^{(n-1)} = \mathbf{A}_{\mathbf{k}+(2,0,0)} + \mathbf{A}_{\mathbf{k}+(0,2,0)} + \mathbf{A}_{\mathbf{k}+(0,0,2)}$ . If the trace vanishes regardless of  $\mathbf{k}$ , the tensor is totally traceless. A totally symmetric tensor which is traceless for some  $\mathbf{k}$  is traceless for all  $\mathbf{k}$  and is said to be totally symmetric and traceless. Similarly, the  $m$ -fold trace is  $\mathbf{A}_{\mathbf{j}}^{(n:m)} = \sum_{|\mathbf{k}|=m} \frac{m!}{\mathbf{k}!} \mathbf{A}_{\mathbf{j}+2\mathbf{k}}$ , where  $j = n - 2m$ .

A totally symmetric tensor  $\mathbf{A}^{(n)}$  can be converted to a totally symmetric traceless tensor  $\mathcal{T}\mathbf{A}^{(n)}$  using the detracer operator  $\mathcal{T}$ . The elements of  $\mathcal{T}\mathbf{A}^{(n)}$  are

$$\begin{aligned} \mathcal{T}[\mathbf{A}^{(n)}]_{\mathbf{n}} &= \sum_{\mathbf{m} \leq \lfloor \mathbf{n}/2 \rfloor} f_{\mathbf{n},\mathbf{m}} \mathbf{A}_{\mathbf{n}-2\mathbf{m}}^{(n:m)} \\ &= \sum_{\mathbf{m} \leq \lfloor \mathbf{n}/2 \rfloor} \left[ f_{\mathbf{n},\mathbf{m}} \sum_{|\mathbf{k}|=m} \frac{m!}{\mathbf{k}!} \mathbf{A}_{\mathbf{n}-2\mathbf{m}+2\mathbf{k}} \right] \end{aligned} \quad (3)$$

where

$$f_{\mathbf{n},\mathbf{m}} = (-1)^m (2n - 2m - 1)!! \frac{\mathbf{n}!}{2^m \mathbf{m}! (\mathbf{n} - 2\mathbf{m})!} \quad (4)$$

The detracer is a linear operator and a projection operator but is

not idempotent ( $\mathcal{T}\mathcal{T} \neq \mathcal{T}$ ). In fact, for  $\mathbf{B}^{(n)} = \mathcal{T}\mathbf{A}^{(n)}$ ,

$$\mathcal{T}\mathbf{B}^{(n)} = (2n-1)!!\mathbf{B}^{(n)} \quad (5)$$

For convenience, we define another operator  $\mathcal{D}\mathbf{A}^{(n)} \equiv \mathcal{T}\mathbf{A}^{(n)}/(2n-1)!!$  that satisfies  $\mathcal{D}\mathcal{D} = \mathcal{D}$ . We should point out that the naming of these operators follows that of Applequist (1989), while Shanker and Huang (2007) use a different convention.

For  $\mathbf{A}^{(n)}$  and  $\mathbf{B}^{(n)}$  totally symmetric there are several useful identities. In particular, the detracer exchange theorem:

$$\mathbf{A}^{(n)} \cdot n \cdot \mathcal{T}\mathbf{B}^{(n)} = \mathcal{T}\mathbf{A}^{(n)} \cdot n \cdot \mathbf{B}^{(n)} \quad (6)$$

and

$$\mathcal{T}\mathbf{A}^{(n)} \cdot n \cdot \mathcal{T}\mathbf{B}^{(n)} = (2n-1)!!\mathbf{A}^{(n)} \cdot n \cdot \mathcal{T}\mathbf{B}^{(n)} \quad (7)$$

which follows from Eq. 5 and Eq. 6. Shanker and Huang (2007) demonstrated that a contraction where at least one tensor is traceless produces a traceless tensor. However, the direct product of a non-traceless tensor with a traceless tensor is not, in general, traceless.

The gradient  $\nabla^n r^{-1}$  is intimately related to  $\mathcal{T}\mathbf{r}^n$ . As early as Maxwell, but then later in Applequist (1984, 1989) and Burgos and Bonadeo (1981), it was shown that

$$\nabla^n r^{-1} = (-1)^n r^{-2n-1} \mathcal{T}[\mathbf{r}^n]_n \quad (8)$$

As we will see, this has important consequences for efficiently computing the electrostatic potential. Using the identity

$$r^{2m} = \sum_{|\mathbf{k}|=m} \mathbf{r}^{2\mathbf{k}} \frac{m!}{\mathbf{k}!} \quad (9)$$

we can write  $\mathcal{T}[\mathbf{r}^n]$  in a compact and computationally efficient form:

$$\mathcal{T}[\mathbf{r}^n]_n = \sum_{\mathbf{m} \leq \lfloor \mathbf{n}/2 \rfloor} f_{\mathbf{n},\mathbf{m}} r^{2\mathbf{m}} \mathbf{r}^{\mathbf{n}-2\mathbf{m}} \quad (10)$$

that contains only a single summation instead of two for the general case (Eq. 3).

### 3. Physical Theory

The  $n$ th-order multipole moment of a distribution  $\rho$  centered at the origin is defined as

$$\boldsymbol{\mu}^{(n)} = \frac{1}{n!} \int_v \rho(\mathbf{s}) \mathbf{s}^n d\mathbf{v} \quad (11)$$

where the integration is over points  $\mathbf{s}$  in a finite volume sphere  $v$ . For any point  $\mathbf{r}$  outside the sphere the potential arising from  $\rho(\mathbf{s})$  is given by the multipole expansion

$$\Phi(\mathbf{r}) = \sum_{n=0}^{\infty} (-1)^n \boldsymbol{\mu}^{(n)} \cdot n \cdot \nabla r^{-1} \quad (12)$$

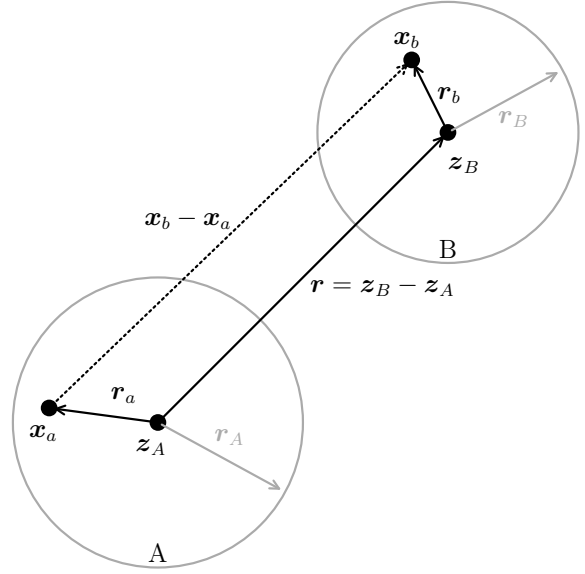


Figure 1: The vectors used in the Taylor expansion of the Green's function  $\phi$  used to compute the potential of a particle at  $\mathbf{x}_a$  in region A at the location  $\mathbf{x}_b$  in region B (Eq. 14).

The potential energy of charge  $q$  at  $\mathbf{r}$  is then  $U(\mathbf{r}) = q\Phi(\mathbf{r})$ . If we now consider a distribution of discrete particles with individual weights  $q_i$  (e.g., charge or mass) generating a potential with the Green's function  $\phi$ , then in distinct, non-overlapping regions  $A, B$ , with centers  $z_A, z_B$  respectively, the total potential at  $\mathbf{x}_b \in B$  from the source particles in A is

$$\Phi_{A \rightarrow B} = \sum_{a \in A} q_a \phi(\mathbf{x}_b - \mathbf{x}_a) \quad (13)$$

In Fig. 1 we sketch the general setup of two interacting regions and the vectors we will need. We define  $\mathbf{r}_a = \mathbf{x}_a - z_A$ ,  $\mathbf{r}_b = \mathbf{x}_b - z_B$ , and  $\mathbf{r} = z_B - z_A$ , so that  $\mathbf{x}_b - \mathbf{x}_a = \mathbf{r} + \mathbf{r}_b - \mathbf{r}_a$ , and the Taylor expansion of  $\phi$  to order  $p$  in both  $\mathbf{r}_a$  and  $\mathbf{r}_b$  is given by the expression

$$\phi \approx \sum_{|\mathbf{m}| \leq p} \sum_{|\mathbf{n}| \leq p-|\mathbf{m}|} \frac{(-1)^{|\mathbf{m}|} \mathbf{r}_a^{\mathbf{m}} \mathbf{r}_b^{\mathbf{n}}}{\mathbf{n}! \mathbf{m}!} \nabla^{\mathbf{n}+\mathbf{m}} \phi(\mathbf{r}) \quad (14)$$

We next pull apart Eq. 13 to define operators (list in Table 1 that allow us to efficiently calculate the potential for all  $A, B$  interacting pairs. These operators are often presented in terms of tensor contractions in the literature but here we use our notation from Sec. 2 to make the implementation clearer. We will further refine and optimize our definitions in the following section. The original derivations of these operators can be found in Shanker and Huang (2007) (although we present a correction to the operator  $M2M$  that maintains the traceless property of the multipole expansion, a crucial point to reducing memory and network communication). Tensors labeled with a bar such as  $\bar{\mathbf{A}}$  are totally symmetric and traceless. When such a tensor is defined, it is understood that only the independent elements of the tensor are stored. Where *dependent* elements are needed, they

Operator	Description	Eq.
P2M	Particle to Multipole expansion	(22)
M2M	Multipole to Multipole recentering	(24)
M2L	Multipole to Local field tensor	(27)
L2L	Local to Local field tensor recentering	(29)
L2P	Local field tensor to Particle	(30)

Table 1: The fast multipole operators described in this article for efficiently calculating long-range interactions of a potential. Their use is sketched in Fig. 2.

are calculated on demand (and reused) from the independent elements of the trace (e.g.,  $\mathbf{A}_{zz} = -\mathbf{A}_{xx} - \mathbf{A}_{yy}$ ).

Consider again two distinct, non-overlapping regions  $A, B$ , each containing a finite number of discrete particles. The traceless multipole expansion for a discrete set of particles in a region  $A$  centered at  $\mathbf{z}$  is given by

$$\bar{\mathbf{M}}_{\mathbf{n}}(\mathbf{z} = \mathbf{x}_a - \mathbf{r}_a) = \mathcal{D}[\mathbf{M}'_{\mathbf{n}}]_{\mathbf{n}} \quad (15)$$

$$\mathbf{M}'_{\mathbf{n}} = \sum_{a \in A} q_a \frac{(-1)^n}{n!} \mathbf{r}_a^{\mathbf{n}} \quad (16)$$

for all  $|\mathbf{n}|$  no greater than the expansion order  $p$ . This is reminiscent of the continuous form in Eq. 11 with change of sign from Eq. 12 absorbed into the definition. Note that the multipole expansion object  $\bar{\mathbf{M}}$  is a polytensor that contains tensors of all rank up to  $p$ .

The field generated by  $A$  at a point  $\mathbf{z}'$  outside  $A$  is described by the local field tensor  $\bar{\mathbf{L}}_{\mathbf{n}}(\mathbf{z}')$ . It is the contraction between  $\bar{\mathbf{M}}$  and  $\nabla^{\mathbf{k}}\phi$  and is only valid outside the volume defining  $\bar{\mathbf{M}}$ : The traceless local field tensor operator ( $M2L$ ) is defined as

$$\bar{\mathbf{L}}_{\mathbf{n}}(\mathbf{z}' = \mathbf{z} + \mathbf{r}) = \sum_{|\mathbf{m}| \leq p - n} \frac{1}{n!} \frac{m!}{\mathbf{m}!} \bar{\mathbf{M}}_{\mathbf{m}}(\mathbf{z}) \nabla^{\mathbf{n}+\mathbf{m}} \phi(\mathbf{r}) \quad (17)$$

From a local field tensor  $\bar{\mathbf{L}}_{\mathbf{n}}(\mathbf{z}')$ , we can approximate the final field (or gradient) at nearby points with the traceless field tensor to particle operator ( $L2P$ ):

$$\nabla^{\mathbf{k}} \Phi(\mathbf{x} = \mathbf{z}' + \mathbf{r}) \approx \sum_{|\mathbf{n}| \leq p - k} \frac{(n+k)!}{k!n!} \frac{n!}{\mathbf{n}!} \mathbf{r}^{\mathbf{n}} \bar{\mathbf{L}}_{\mathbf{n}+\mathbf{k}}(\mathbf{z}') \quad (18)$$

for some  $\mathbf{x}$  in  $B$  centered at  $\mathbf{z}'$ . Substituting Eq. 15 and Eq. 17 into Eq. 18 simplifies to the original expression Eq. 13 for  $\Phi_{A \rightarrow B}$ . The power of these operators is clear when one considers that field tensors from multiple non-overlapping regions may be accumulated (i.e., summed element-wise) to form a new field tensor if the centers are the same. With such a field tensor,  $L2P$  simultaneously applies the affect of multiple regions in a single step.

Finally, for the fast multipole method to be fully  $O(N)$  we need two more operators. Since our choice of multipole expansion center in  $P2M$  was arbitrary, we can choose to take a different center. The operator  $M2M$  recenters an existing traceless

multipole about a new point  $\mathbf{z}'$ :

$$\bar{\mathbf{M}}_{\mathbf{n}}(\mathbf{z}' = \mathbf{z} - \delta) = \mathcal{D}[\mathbf{M}'_{\mathbf{n}}]_{\mathbf{n}} \quad (19)$$

$$\mathbf{M}'_{\mathbf{n}} = \sum_{|\mathbf{k}| \leq |\mathbf{n}|} \frac{(-1)^k}{k!} \left[ \frac{k!}{\mathbf{k}!} \frac{(n-k)!}{(\mathbf{n}-\mathbf{k})!} \frac{\mathbf{n}!}{n!} \right] \delta^{\mathbf{k}} \bar{\mathbf{M}}_{\mathbf{n}-\mathbf{k}}(\mathbf{z}) \quad (20)$$

If two different multipole expansions share the same center they may be combined into a single expansion. The factor in brackets ensures that the direct product between  $\delta^{\mathbf{k}}$  and  $\bar{\mathbf{M}}$  produces a symmetric result that can be stored in the compressed tensor format. Similarly, the traceless field tensor translation operator ( $L2L$ )

$$\bar{\mathbf{L}}_{\mathbf{n}}(\mathbf{z}' = \mathbf{z} + \delta) = \sum_{|\mathbf{k}| \leq p - n} \frac{(n+k)!}{n!k!} \frac{k!}{\mathbf{k}!} \delta^{\mathbf{k}} \bar{\mathbf{L}}_{\mathbf{n}+\mathbf{k}}(\mathbf{z}) \quad (21)$$

moves the location where a field tensor was evaluated. As with the multipole expansion, two field tensors sharing the same center may be combined.

It should also be noted that  $P2M$  is nothing more than an application of  $M2M$ . In this case the original expansion of the particle is nothing more than the monopole shifted from the enclosing volume's center to the particle position. This idea is useful when one considers dipoles as discussed in Sec. 4.1.

Fig. 2 sketches the hierarchical application of each operator to compute the interaction of two large regions on a third. Multipole expansions for the particles in the smallest regions are computed using  $P2M$  and combined to larger multipole expansions with  $M2M$ . Interactions between larger regions are evaluated by computing the local field tensor using  $M2L$ . This field expansion is then recentered at smaller local regions using  $L2L$  and finally evaluated at particle position with  $L2P$ .

## 4. Improved Operators

As we stated earlier, our presentation of the FMM operators in the previous section provides a standard, familiar foundation, which is applicable to any Green's function. Taken individually, the operators are all correct and can stand on their own. If we consider the operators all together in a single framework, a number of numerical improvements can be made by modifying our definitions. These modifications retain the correctness of the final potential, but break the correctness of the individual operators. By choosing to do this, we can reduce the number of operations in the final code. In our final formulation, we also provide an efficient form of the  $M2M$  recentering operator that also correctly preserves the traceless property of the multipole tensor.

At this point, we substitute the important case  $\phi(\mathbf{r} = \mathbf{x}_b - \mathbf{x}_a) = |\mathbf{r}|^{-1}$  found in molecular dynamics or gravity calculations to take advantage of the traceless tensor form in Eq. 8.

*Operator P2M (Particle to traceless multipole):* The traceless multipole tensor for particles in an enclosed region  $A$  now takes

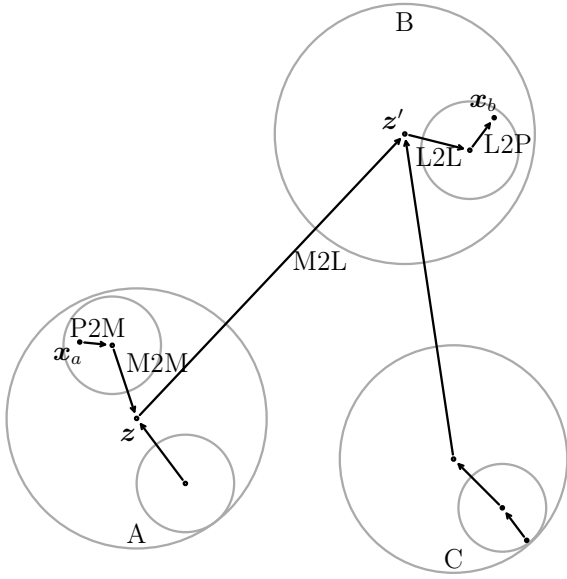


Figure 2: A sketch of the FMM operators used to map the potential of particles in regions A, C to particles located in region B. By using the *M2L* operator to compute the local field tensor due to multiple regions at the same point in region B the effect of all the particles in those two regions can be combined into a single local field tensor. This field tensor is used to compute the final potential of particles in B.

the form

$$\bar{\mathbf{M}}_n(\mathbf{z} = \mathbf{x}_a - \mathbf{r}_a) = \sum_{a \in A} q_a \mathcal{D}[\mathbf{M}'_n] \quad (22)$$

$$\mathbf{M}'_n = -\mathbf{r}_a^n \quad (23)$$

where  $\mathbf{z}$  is the region center and  $q_a, \mathbf{x}_a$  are the charge and position of a particle  $a \in A$ , respectively. The detracer  $\mathcal{D}$  can be moved inside the summation and  $q_a$  and  $1/n!$  outside the detracer because  $\mathcal{D}$  is a linear operator. The factorial then vanishes by absorbing  $n!$  from *M2L* and *M2M*.

*Operator M2M (Traceless multipole with shifted center):* The *M2M* operator shifts the expansion center of an existing traceless multipole expansion to a new location  $\mathbf{z}'$ :

$$\bar{\mathbf{M}}_n(\mathbf{z}' = \mathbf{z} - \delta) = \mathcal{D}[\mathbf{M}'_n] \quad (24)$$

$$\mathbf{M}'_n(\mathbf{z}') = \sum_{|\mathbf{k}| \leq n} \frac{n!}{\mathbf{k}!(\mathbf{n} - \mathbf{k})!} (-\delta)^{\mathbf{n} - \mathbf{k}} \bar{\mathbf{M}}_{\mathbf{k}}(\mathbf{z}) \quad (25)$$

The factor of  $n!/\mathbf{k}!$  accounts for the fact that the tensor product of  $\delta$  with  $\bar{\mathbf{M}}$  must be made symmetric<sup>1</sup>. The result is still not traceless, hence the application of the detracer. Here we also see the usefulness of defining  $\mathcal{D}$ , so that multiple applications of *M2M* do not introduce factors of  $(2n - 1)!!$ .

<sup>1</sup>It is tempting to remove this by absorbing  $\mathbf{k}!$  into the definition of  $\bar{\mathbf{M}}$ . However, if  $\bar{\mathbf{M}}$  is traceless this will break the harmonic property (consider for  $\mathbf{k} = (0, 0, 3)$  that  $\mathbf{M}_{zzz}/3! = -(\mathbf{M}_{xxz} + \mathbf{M}_{yyz})/3! \neq -(\mathbf{M}_{xxz}/2! + \mathbf{M}_{yyz}/2!)$ ). One can work around this, but the resulting calculation outweighs the extra multiplications.

Inserting Eq. 25 into Eq. 24, expanding the detracer, and rearranging terms we arrive at

$$\bar{\mathbf{M}}_n(\mathbf{z}' = \mathbf{z} - \delta) = \bar{\mathbf{M}}_0(\mathbf{z}) \mathcal{T}[-\delta^n]_n + \frac{1}{(2n - 1)!!} \times \left[ \sum_{1 \leq |\mathbf{q}| \leq n} \frac{\bar{\mathbf{M}}_{\mathbf{q}}(\mathbf{z})}{\mathbf{q}!} \sum_{\mathbf{m} \leq \lfloor \mathbf{n}/2 \rfloor} f_{\mathbf{n}, \mathbf{m}} \sum_{|\mathbf{k}| = \mathbf{m}} \frac{m!}{\mathbf{k}!} \frac{(\mathbf{j} + \mathbf{q})!}{\mathbf{j}!} \mathcal{T}[-\delta^{\mathbf{j}}]_{\mathbf{j}} \right] \quad (26)$$

where  $\mathbf{j} = \mathbf{n} + 2\mathbf{k} - 2\mathbf{m} - \mathbf{q}$  and the traceless tensor  $\mathcal{T}[\delta^{\mathbf{s}}]$  has been substituted. This substitution is allowed because of the later tensor contraction with  $\nabla \mathbf{r}^{-1}$ , which is traceless, in *M2L* where only independent terms are needed. This longer form for *M2M* translates well into efficient code, where the factorials are precalculated and reduce to constants.

*Operator M2L (Traceless local field tensor):* The local field tensor

$$\bar{\mathbf{L}}_n(\mathbf{z}' = \mathbf{z} + \mathbf{r}) = \sum_{|\mathbf{m}| \leq p - n} \frac{1}{\mathbf{m}!} \bar{\mathbf{M}}_{\mathbf{m}}(\mathbf{z}) \bar{\mathbf{D}}_{\mathbf{n} + \mathbf{m}}(\mathbf{r}) \quad (27)$$

describes the potential field produced by a multipole expansion  $\bar{\mathbf{M}}(\mathbf{z})$  at a local point  $\mathbf{z}'$ . It is only valid outside the radius defining  $\bar{\mathbf{M}}$ . Here we use Eq. 8 to express the traceless gradient as

$$\bar{\mathbf{D}}_{\mathbf{k}}(\mathbf{r}) = \nabla^{\mathbf{k}} \mathbf{r}^{-1} = (-1)^{\mathbf{k}} \mathbf{r}^{-2\mathbf{k} - 1} \mathcal{T}[\mathbf{r}^{\mathbf{k}}]_{\mathbf{k}} \quad (28)$$

*Operator L2L (Traceless local field tensor translation):* As with the multipole, we can also choose to change where we measure the field tensor  $\bar{\mathbf{L}}$ . This shifting operator takes the following form

$$\bar{\mathbf{L}}_n(\mathbf{z}' = \mathbf{z} + \delta) = \sum_{|\mathbf{k}| \leq p - n} \frac{\delta^{\mathbf{k}}}{\mathbf{k}!} \bar{\mathbf{L}}_{\mathbf{n} + \mathbf{k}}(\mathbf{z}) \quad (29)$$

*Operator L2P: (Traceless local field tensor to particle):* Finally, when we want to evaluate the potential (or force, or electric field, etc.) we need only shift the field tensor to the location of the particle and examine the appropriate tensor components:

$$\nabla^{\mathbf{n}} \Phi(\mathbf{x} = \mathbf{z} + \mathbf{r}) \approx \bar{\mathbf{L}}_n(\mathbf{x}) \quad (30)$$

From our definitions, the potential is defined to be positive. For astrophysical applications, the potential and respective gradients should be negated.

#### 4.1. Dipoles and higher order multipoles

Some applications in molecular dynamics also include point dipoles  $\mathbf{p}$  in addition to single point charges. The dipoles capture the polarization effect present in water and many other molecules. Dipoles have a net charge of zero, but generate and respond to electric fields as though they were two opposite charged particles infinitely close together. They can be incorporated into the FMM framework in a straightforward manner by modifying the construction of the multipole. The multipole construction in Eq. 22 is nothing more than a sum over monopoles  $\mathbf{M}_0 = q_a$  at  $\mathbf{x}_a = 0$  that have been shifted by  $\mathbf{r}_a$  with the shifting operator Eq. 24. Likewise, we can construct point

dipoles at  $\mathbf{r}_a$  by shifting a pure dipole  $\mathbf{M}_1^{\text{dipole}} = \mathbf{p}$ , where all other components are zero. Higher order constructions are similarly possible, but one must be careful that the multipole object is symmetric and traceless before shifting.

## 5. Code Generator

The computer code for the FMM operators was generated automatically by a Python program based on the symbolic algebra library Sympy (Meurer et al., 2017). Routines for each expansion order  $p$  are generated separately ( $p$  is not a parameter to the routines), but there is no limit to which order can be chosen. By choosing to hard-code routines for particular values of  $p$  we can generate more efficient, compact code. The program currently outputs code in Fortran, but can easily generate any other language.

The optimizing phase reduces the number of mathematical operations by extracting common subexpressions within an operator to intermediate variables and factoring out common constants. All factorials (particularly, for instance, in M2M) are precomputed and become simple constant coefficients within the expressions. Furthermore, we can reorder the code to improve memory accesses. On average, we see a 70% reduction of operations in the M2L operator, for instance. Most importantly, in our empirical studies discussed in Sec. 7, the scaling as a function of  $p$  is drastically improved by the optimizer.

There are no loops in the final code. This can make it difficult for an optimizing compiler to take advantage of vector instructions, which would use these instructions to compute multiple successive iterations simultaneously. However, it is often the case in FMM implementations that one can compute the interaction of many multipoles at one time. Therefore, we generate routines that accept multiple packed tensors and vectorized code to process them. Instead of computing successive iterations of a loop simultaneously for a single tensor, pairs of tensors are computed in parallel. This achieves a 1.8x speedup for  $p = 7$  on vector instructions that process two double length floating point numbers (the speed-up is less than 2x due to the packing/unpacking of the tensors). On newer processors that support vector instructions for four simultaneous doubles, new routines are simple to generate.

## 6. The Fast Multipole Method

Having defined the operators we need, we now describe the fast multipole method and when we use the operators. Our FMM implementation is based on the tree code method discussed in Dehnen (2002); Yokota and Barba (2012), and Coles and Masella (2015). We refer the reader again to a sketch of the procedure in Fig. 2.

We decompose the potential  $\Phi^{\text{tot}} = \Phi^{\text{near}} + \Phi^{\text{far}}$  into near and far components that will be handled separately. The near field is computed using a direct sum  $O(n^2)$  method, where  $n \ll N$  is small and does not change with the total system size  $N$ , so that we can consider it a constant cost.

The volume of  $N$  particles is hierarchically decomposed into a binary tree of nested cells with the smallest (leaf) cells having no more than  $N_{\text{bucket}} (\approx 32)$  particles. Cells are divided across the longest axis such that there are an equal number of particles on each side. For a perfectly balanced tree there are  $N_{\text{cells}} = 2N/N_{\text{bucket}} - 1 \rightarrow O(N)$  cells. In each of the smallest cells we calculate a multipole expansion with  $P2M$  from Eq. 22. Working from the bottom up, we can efficiently compute the multipole expansion of a parent cell (with center  $\mathbf{z}_P$ ) by recentering each child cell expansion to  $\mathbf{z}_P$  with  $M2M$  from Eq. 24 and summing the components. This is an  $O(N)$  operation for the whole tree.

The interaction phase decides for which cell pairs a multipole interaction is performed according to our multipole acceptance criteria (MAC). Cells further apart will produce a more accurate result. Furthermore, the larger the regions we can use, the less we need to compute before we have covered the entire volume. We use the following MAC, with tuning parameter  $0 \leq \theta \leq 1$ , to decide whether two regions are sufficiently far part: If  $\theta|\mathbf{z}_B - \mathbf{z}_A| > |\mathbf{r}_A + \mathbf{r}_B|$  is satisfied for region centers  $\mathbf{z}_A, \mathbf{z}_B$  with respective radii  $\mathbf{r}_A, \mathbf{r}_B$  then the mutual interaction is allowed, otherwise we must split the regions into smaller pieces and compare those (see Fig. 1). Note that for  $\theta = 0$  no two regions will be accepted and the method will degrade to an  $O(N^2)$  direct summation over the entire volume.

Using the dual-tree walk algorithm from Dehnen (2002) we begin at the root cell where we apply the MAC to the two child cells. If this is satisfied, we can compute the mutual interactions  $\bar{\mathbf{L}}_{A \rightarrow B}$  and  $\bar{\mathbf{L}}_{B \rightarrow A}$  using  $M2L$  from Eq. 27 in both directions. The resulting field tensors are accumulated at each respective cell. Also note that this mutual interaction implies that Newton's third law is satisfied and linear momentum is conserved. If the MAC is not satisfied, the algorithm is recursively applied, with each child of the larger cell compared to the smaller cell. If a cell to be expanded is a leaf cell, the other cell of the interaction is expanded instead. If two cells on the lowest level do not satisfy the MAC then the interaction is considered part of the near field component and is computed via a direct summation. By cutting off the tree decent with the MAC and computing the cell-cell interactions, this phase runs in  $O(N)$  time.

It is during this phase that a distributed implementation of FMM may exchange multipole expansion data. With the traceless tensors, this data exchange is minimized.

The field tensors that have been accumulated and stored throughout the tree are then translated to the lowest cell level to compute the final field at each particle position. This is again an  $O(N)$  process. Starting from the root cell and descending depth-first to the lowest cells, the field tensor at each cell is re-centered using  $L2L$  from Eq. 29 on each of its child cells and accumulated.

The final field tensor at the center of each leaf cell represents the total potential from all other cells. The potential (or gradients) at each particle position is then computed using  $L2P$  in Eq. 30. Since this phase simply loops over all particles it is also an  $O(N)$  process.

In terms of the number of applications of  $M2M$ , the bottom-up construction of the multipole expansions in each tree cell is

Operator	$p = 3$		$p = 5$		$p = 7$	
P2M	40	<i>24</i>	132	<i>79</i>	347	<i>230</i>
M2M	211	<i>31</i>	1308	<i>411</i>	6007	<i>2375</i>
M2L	214	<i>119</i>	987	<i>701</i>	3158	<i>2553</i>
L2L	122	<i>86</i>	520	<i>454</i>	1404	<i>1298</i>
L2P	123	<i>72</i>	426	<i>256</i>	887	<i>586</i>

Table 2: The number of floating point operations (FLOPs) generated for each of the five multipole routines used in the molecular dynamics program Polaris(MD) for common expansion orders. The routines are generated and optimized using a symbolic algebra library but these numbers only represent an upper bound. Hand optimization of the routines, or improvements to the library, may yield lower numbers. *Italics*: The number of FLOPs generated for a gravity calculation that only computes the gradient of the potential and assumes the dipole vanishes.

strictly  $O(N_{\text{cells}})$  without any hidden constants. However, for the interaction phase the number of calls to *M2L* will be dependent on the geometry of the problem. In realistic scenarios, *M2L* is used far more than *M2M*, often by 40–60 times as measured in our experiments.

## 7. Discussion and Analysis

For each operator, the code generator reports the number of floating-point operations used (additions, multiplication, etc.). In Table 2 we list this information for expansion orders  $p = 3, 5, 7$  in both the electrostatic and gravitational cases. For many electrostatic simulations where cells may be charge neutral, and the expansion dominated by the dipole term, an expansion order up to  $p = 7$  is necessary to achieve an accurate calculation. Astrophysical applications do not suffer from this issue as the mass must always be positive and the multipole expansion is already reasonably accurate at low order, although some implementations of FMM for astrophysics do use  $p = 5$ . In gravity codes, the expansion is typically located at the center of mass, which we assume here. This causes the dipole to vanish and reduces the number of operations in the higher order tensor terms. Furthermore, only the gradient of the potential  $\nabla\Phi$  is required, removing the need for the potential and hessian to be calculated.

The numbers presented here are for reference only and should not be interpreted as the minimal number of operations. Hand optimization can lead to a further reduction and future improvements to the code generator may also be possible. The code generator does, however, allow for a greater flexibility and experimentation with the form of the operators and easy switching between application requirements.

In Fig. 3 we show the effect of running the symbolic code optimizer over the generated operators. Recall that the optimizer extracts common subexpressions into temporary variables and performs other mathematical reductions. In the top plot we show the relative reduction in size (operation count) after optimizing the non-traceless operators. Most notable is the significant reduction of *M2L*, which we attribute to the optimizer effectively finding the symmetries that are made explicit in the traceless version. Indeed, the relative reduction is far less in the

second plot, simply because the original traceless expression is itself already more efficient. In the bottom plot we compare the optimized versions of the traceless and non-traceless operators. Here we see that *M2M* is heavier in the traceless version due to the detracer, but since *M2M* is used far less than the most used operator *M2L*, we still see a net improvement in efficiency. For instance, in the molecular dynamics code Polaris(MD), *M2L* is called 40x more than *M2M*. This increases to 60x when one disables the polarization routines (and so would be more similar to astrophysics codes).

In Fig. 4 we show the general scaling trends of the operation count as a function of expansion order. We fit each of these curves over  $5 \leq p \leq 10$  with a simple exponential to determine an empirical scaling. In Fig. 5 we compare these scaling values with the unoptimized operators and the non-traceless operators. We can clearly see the effect of using the traceless versions on improving the scaling. Perhaps more interesting is that the optimization also changes the scaling compared with the unoptimized version. One may have expected that optimization would reduce the overall number of operations but not change the scaling trend. We attribute this to the optimizer identifying (although not knowingly) further symmetries in the equations that can be exploited.

In addition to the operation count, we ran timing tests to measure the average time to perform a single operator in isolation (outside of any simulation environment). The scaling plots are shown in Fig. 6.

In-situ tests were also performed to demonstrate the real effect of using traceless tensors. Three non-hydrated subsets of the HIV-1 capsid system were considered with 21,612 atoms, 43,244 atoms, and 86,448 atoms, respectively. These systems were previously used in performance testing of our serial FMM implementation (Coles and Masella, 2015). Here we use a parallel FMM strategy which will be reported on in an upcoming publication. For each system, 1000 simulation steps were performed on up to 28 cores. In Fig. 7 we show the average speed-up of the traceless version over the non-traceless one as a function of total core count. We should stress that these routines are producing the same numerical results as expected.

## 8. Summary and Outlook

We have demonstrated fully traceless operators for the fast multipole method (FMM) in a form that transfers well to computer code and developed a code generator to produce an optimized implementation. Traceless multipole tensors reduce the memory requirements by nearly 50% for an expansion order  $p = 7$ . Such an expansion order is necessary in sensitive electrostatic simulations of molecular dynamics. The traceless multipole operators are currently used in Polaris(MD), a highly parallel and distributed molecular dynamics package.

We evaluated the performance in isolated and in-situ tests and compared our results to non-traceless operators. For our test applications of biophysical systems, we find a  $\sim 20\%$  improvement of the FMM interaction phase (see Fig. 7). We also find that the detracer operator from Applequist (1989), used to

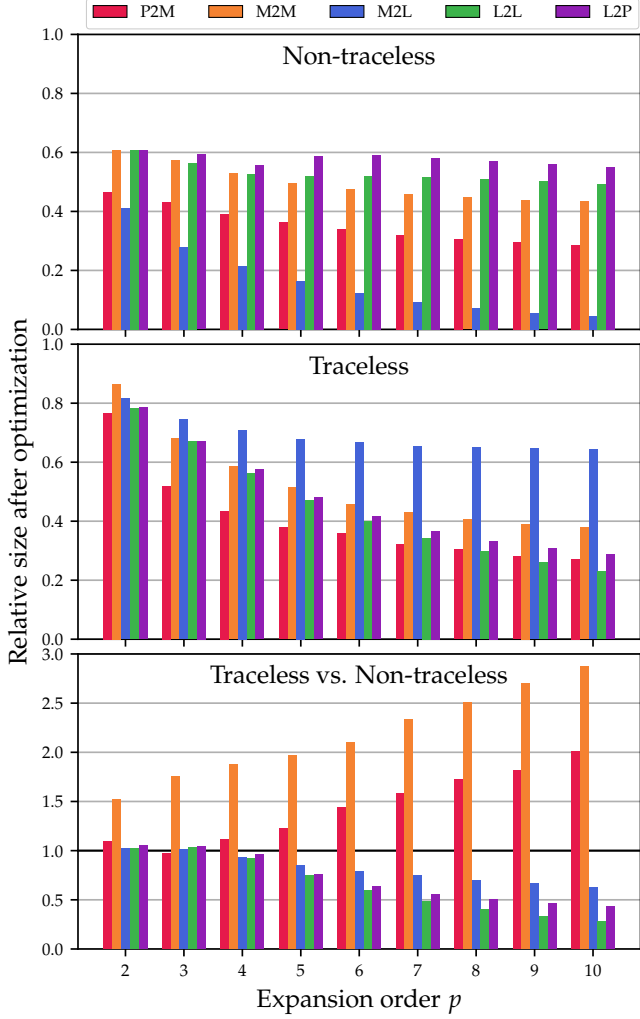


Figure 3: *Top*: The relative size (operation count) of the non-traceless operators after running the code optimizer for different expansion orders. The significant reduction of  $M2L$  can be attributed to the optimizer finding symmetries that are explicitly exposed in the traceless version. *Center*: The relative size for the traceless operators. *Bottom*: The reduced size of the traceless operators compared to the non-traceless operators, both after optimization. While the traceless  $M2M$  is much heavier, it is used  $\sim 40x$  less frequently than the most used operator  $M2L$ , resulting in a net efficiency increase.

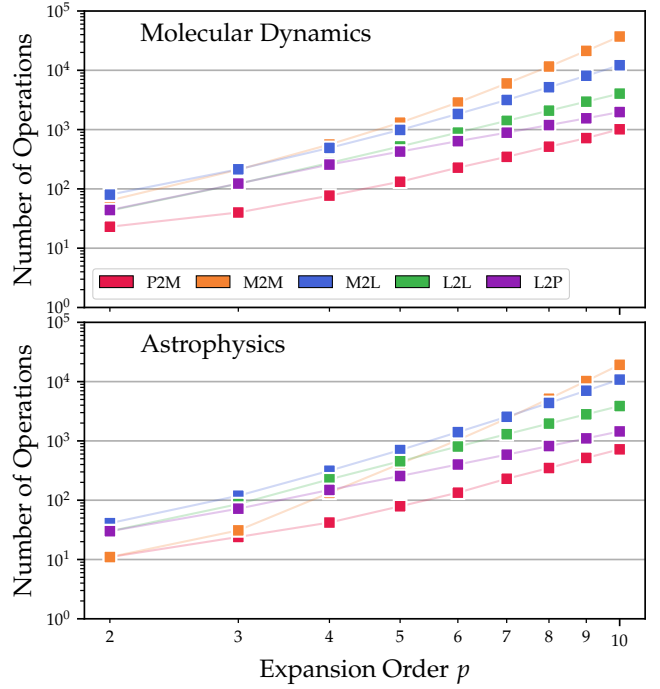


Figure 4: The number of floating-point operations generated for each optimized FMM routine as a function of the expansion order  $p$ . *Top*: The molecular dynamics case where all terms of the multipole expansion are calculated and, in the case of  $L2P$ ,  $\Phi$ ,  $\nabla\Phi$ , and  $\nabla^2\Phi$  are calculated. *Bottom*: The astrophysics case, where the operators assume the dipole term vanishes and  $L2P$  only computes the gradient (acceleration)  $\nabla\Phi$ .

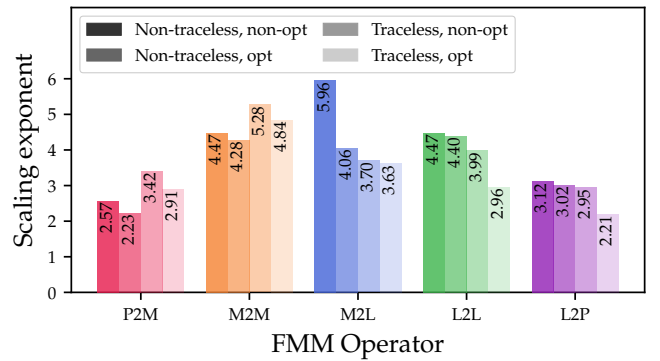


Figure 5: The effectiveness of the code optimizer in improving the scaling efficiency of the FMM operators for MD. We plot the scaling exponents for each of the FMM operators derived by fitting the number of FLOPs for each operator over expansion orders  $5 \leq p \leq 10$ . We show four variants of an operator: 1) The non-traceless, unoptimized version, 2) the non-traceless version after running the symbolic code optimizer, 3) the traceless, unoptimized version, and 4) the traceless, optimized version currently used in production (and shown in Fig. 4).

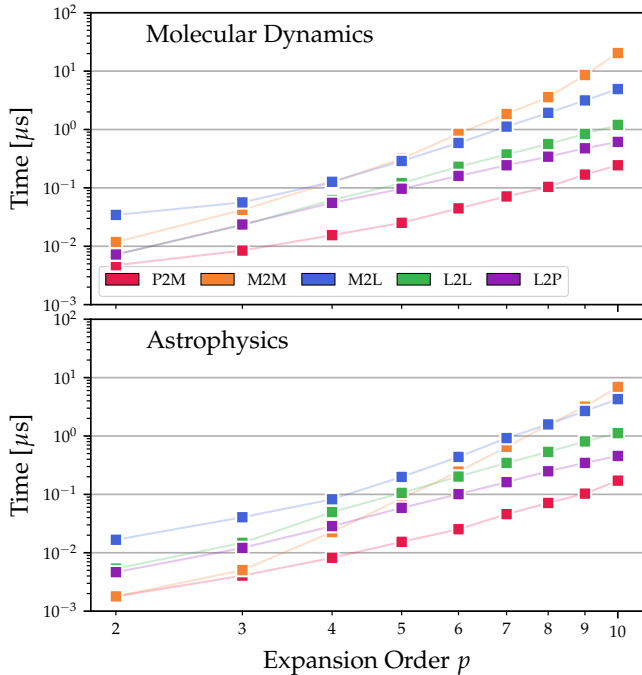


Figure 6: Average time in microseconds to run each operator as a function of expansion order  $p$ . Top and bottom figures are as in Fig. 4.

construct the traceless tensors, does not heavily affect the performance of the final code as suggested in Huang et al. (2018), but rather serves to improve the final performance.

We have also developed a code generator based on a symbolic algebra library, and have shown that efficient implementations of the traceless operators can be generated and optimized automatically to any order. For applications to FMM kernels where the Green’s function is not harmonic (and the traceless formulation is not possible), this method could also be used to produce more efficient software. The symbolic approach has allowed us to programmatically verify the correctness of the code and to count the number of mathematical operations.

The optimized code shows improved scaling compared with the naive approach. Fitting the optimized operation count for expansion orders up to  $p = 10$ , we have found that, empirically, the M2M operator scales  $< \mathcal{O}(p^5)$ ; P2M, L2L, L2P as  $< \mathcal{O}(p^3)$ ; and M2L as  $< \mathcal{O}(p^4)$ .

The reduced memory footprint is important for highly distributed implementations of FMM, which need to limit the amount of data communication. With the higher core count found on modern computing servers, reduced memory requirements also allow a larger fraction of a problem to be stored and processed locally. Specialized versions that use graphics processing units (GPUs) can also benefit in a similar way, where the bottleneck is often in the data transfer to and from the GPU. Implementations of the fast multipole method based on our formulation will be well suited for current and future technology.

## 9. Acknowledgements

JPC would like to thank Walter Dehnen for several lively and educational discussions. The authors also thank Martin Zacharias and Michel Masella for their comments on this manuscript. Parallel scaling tests were performed on the SuperMUC cluster at the Leibniz-Rechenzentrum in Garching, Germany. Other performance tests were conducted on the in-house cluster of the Lehrstuhl für Theoretische Biophysik at TUM.

## Appendix A. Multi-index Notation

Multi-index notation simplifies the presentation of symmetric tensors. In this article tensors (resp. indices) are three dimensional, but the notation can easily be extended to any number of dimensions. For index  $\mathbf{n} = (n_x, n_y, n_z)$ , where  $n_i \geq 0$ , the  $\mathbf{n}$ th index of tensor  $\mathbf{A}$  is  $\mathbf{A}_{\mathbf{n}}$ . Occasionally, a different notation may be used to refer to specific indices of a three-dimensional tensor. For instance, we may write  $\mathbf{A}_{xyzzz} = \mathbf{A}_{(1,2,3)}$ , or  $\mathbf{A}_{xxz} = \mathbf{A}_{(2,0,1)}$ . In the following examples,  $\mathbf{n}$  and  $\mathbf{m}$  are indices with three dimensions,  $\mathbf{r}$  is a vector, and  $k$  a scalar. Index tuples with negative components do not exist and any expressions containing such indices are to be ignored. In short, we use the following definitions:  $|\mathbf{n}| \equiv n_x + n_y + n_z$ ;  $\mathbf{n}! \equiv n_x! n_y! n_z!$ ;  $\mathbf{n} \pm k \equiv (n_x \pm k, n_y \pm k, n_z \pm k)$ ;  $\mathbf{n} \pm \mathbf{m} \equiv (n_x \pm m_x, n_y \pm m_y, n_z \pm m_z)$ ;  $\mathbf{r}^{\mathbf{n}} \equiv r_x^{n_x} r_y^{n_y} r_z^{n_z}$ .

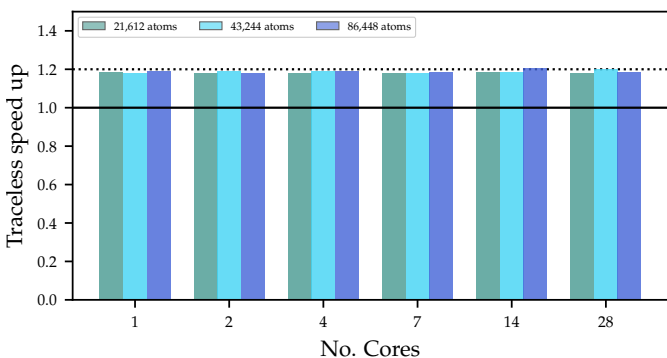


Figure 7: Average speedup of the parallel FMM interaction phase when using traceless multipole tensors with an expansion order of  $p = 7$  compared to the non-traceless version. Measurements were made over 1000 steps of three HIV-1 capsid subsets of increasing size.

## Appendix B. Tensor Storage

For reference, Table B.3 lists the number of elements required for traceless and non-traceless tensors, as well as the fraction of space saved in using the traceless version.

$p$	Non-traceless		Traceless		Savings (%)
	at $p$ th order	total elements	at $p$ th order	total elements	
0	1	1	1	1	0
1	3	4	3	4	0
2	6	10	5	9	10
3	10	20	7	16	20
4	15	35	9	25	29
5	21	56	11	36	36
6	28	84	13	49	42
7	<b>36</b>	<b>120</b>	<b>15</b>	<b>64</b>	<b>47</b>
8	45	165	17	81	51
9	55	220	19	100	55
10	66	286	21	121	58

Table B.3: Storage size needed for non-traceless and traceless multipole tensors for expansion orders  $p \leq 10$ . For production molecular dynamics runs we use an expansion order  $p = 7$ . The last column shows by how much the storage is reduced when using the traceless operator. This has important consequences for memory storage and network communication.

## Appendix C. Technical Details

The multipole generating software was written using Python v2.7.13 and Sympy v1.1.1. Operator timing tests shown in Fig. 6 were performed on an Intel Sandybridge 2.60 GHz E5-2640v3 CPU. Speedup tests in Fig. 7 were run on an Intel Haswell E5-2697v3 CPU running at 1.8 GHz.

## References

Applequist, J., 1984. Fundamental relationships in the theory of electric multipole moments and multipole polarizabilities in static fields. *Chemical Physics* 85, 279 – 290. doi:[https://doi.org/10.1016/0301-0104\(84\)85039-9](https://doi.org/10.1016/0301-0104(84)85039-9).

Applequist, J., 1989. Traceless cartesian tensor forms for spherical harmonic functions: new theorems and applications to electrostatics of dielectric media. *Journal of Physics A: Mathematical and General* 22, 4303.

Barnes, J., Hut, P., 1986. A hierarchical  $O(N \log N)$  force-calculation algorithm. *Nature* 324, 446–449. doi:[10.1038/324446a0](https://doi.org/10.1038/324446a0).

Burgos, E., Bonadeo, H., 1981. Electrical multipoles and multipole interactions: compact expressions and a diagrammatic method. *Molecular Physics* 44, 1–15. doi:[10.1080/00268978100102251](https://doi.org/10.1080/00268978100102251), arXiv:<https://doi.org/10.1080/00268978100102251>.

Coles, J.P., Masella, M., 2015. The fast multipole method and point dipole moment polarizable force fields. *J. Chem. Phys.* 142, 024109.

Darden, T., York, D., Pedersen, L., 1993. Particle mesh Ewald: An  $N \cdot \log(N)$  method for Ewald sums in large systems. *J. Chem. Phys.* 98, 10089–10092. doi:[10.1063/1.464397](https://doi.org/10.1063/1.464397).

Dehnen, W., 2002. A Hierarchical  $O(N)$  Force Calculation Algorithm. *Journal of Computational Physics* 179, 27–42. doi:[10.1006/jcph.2002.7026](https://doi.org/10.1006/jcph.2002.7026).

Dehnen, W., 2014. A fast multipole method for stellar dynamics. *Computational Astrophysics and Cosmology* 1, 1. doi:[10.1186/s40668-014-0001-7](https://doi.org/10.1186/s40668-014-0001-7).

Greengard, L., Rokhlin, V., 1987. A fast algorithm for particle simulations. *Journal of Computational Physics* 73, 325–348. doi:[10.1016/0021-9991\(87\)90140-9](https://doi.org/10.1016/0021-9991(87)90140-9).

Greengard, L.F., Huang, J., 2002. A new version of the fast multipole method for screened coulomb interactions in three dimensions. *Journal of Computational Physics* 180, 642 – 658. doi:<https://doi.org/10.1006/jcph.2002.7110>.

Huang, H., Luo, L.S., Li, R., Chen, J., Zhang, H., 2018. Improve the efficiency of the cartesian tensor based fast multipole method for coulomb interaction using the traces. *Journal of Computational Physics* 371, 122 – 136. doi:<https://doi.org/10.1016/j.jcp.2018.05.028>.

Lorenzen, K., Schwörer, M., Tröster, P., Mates, S., Tavan, P., 2012. Optimizing the accuracy and efficiency of fast hierarchical multipole expansions for md simulations. *Journal of Chemical Theory and Computation* 8, 3628–3636. doi:[10.1021/ct300080n](https://doi.org/10.1021/ct300080n).

Masella, M., Borgis, D., Cuniasse, P., 2008. Combining a polarizable force-field and a coarse-grained polarizable solvent model: Application to long dynamics simulations of bovine pancreatic trypsin inhibitor. *Journal of Computational Chemistry* 29, 1707–1724. doi:[10.1002/jcc.20932](https://doi.org/10.1002/jcc.20932).

Masella, M., Borgis, D., Cuniasse, P., 2011. Combining a polarizable force-field and a coarse-grained polarizable solvent model. ii. accounting for hydrophobic effects. *Journal of Computational Chemistry* 32, 2664–2678. doi:[10.1002/jcc.21846](https://doi.org/10.1002/jcc.21846).

Masella, M., Borgis, D., Cuniasse, P., 2013. A multiscale coarse-grained polarizable solvent model for handling long tail bulk electrostatics. *Journal of Computational Chemistry* 34, 1112–1124. doi:[10.1002/jcc.23237](https://doi.org/10.1002/jcc.23237).

Meurer, A., Smith, C.P., Paprocki, M., Čertík, O., Kirpichev, S.B., Rocklin, M., Kumar, A., Ivanov, S., Moore, J.K., Singh, S., Rathnayake, T., Vig, S., Granger, B.E., Muller, R.P., Bonazzi, F., Gupta, H., Vats, S., Johansson, F., Pedregosa, F., Curry, M.J., Terrel, A.R., Roučka, v., Saboo, A., Fernando, I., Kulal, S., Cimrman, R., Scopatz, A., 2017. Sympy: symbolic computing in python. *PeerJ Computer Science* 3, e103. URL: <https://doi.org/10.7717/peerj-cs.103>, doi:[10.7717/peerj-cs.103](https://doi.org/10.7717/peerj-cs.103).

Shanker, B., Huang, H., 2007. Accelerated cartesian expansions – a fast method for computing of potentials of the form  $r$  for all real  $r$ . *Journal of Computational Physics* 226, 732 – 753. doi:<https://doi.org/10.1016/j.jcp.2007.04.033>.

Yokota, R., Barba, L.A., 2012. A tuned and scalable fast multipole method as a preeminent algorithm for exascale systems. *Int. J. High Perform. Comput. Appl.* 26, 337–346. doi:[10.1177/1094342011429952](https://doi.org/10.1177/1094342011429952).